

Combined Use of Satellite Observations and Global Hawk Unmanned Aircraft Dropwindsondes for Improved Tropical Cyclone Analyses and Forecasts

HUI CHRISTOPHERSEN

Cooperative Institute for Marine and Atmospheric Studies, University of Miami, and NOAA/Atlantic Oceanographic and Meteorological Laboratory/Hurricane Research Division, Miami, Florida

ROBERT ATLAS

NOAA/Atlantic Oceanographic and Meteorological Laboratory, Miami, Florida

ALTUG AKSOY AND JASON DUNION

Cooperative Institute for Marine and Atmospheric Studies, University of Miami, and NOAA/Atlantic Oceanographic and Meteorological Laboratory/Hurricane Research Division, Miami, Florida

(Manuscript received 9 November 2017, in final form 4 June 2018)

ABSTRACT

This study demonstrates that Global Hawk unmanned aircraft system dropwindsondes and Atmospheric Infrared Sounder (AIRS) observations can be complementary in sampling a tropical cyclone (TC). The assimilation of both datasets in a regional ensemble data assimilation system shows that the cumulative impact of both datasets is greater than either one alone because of the presence of mutually independent information content. The experiment that assimilates both datasets has smaller position and intensity errors in the mean analysis than those with individual datasets. The improvements in track and intensity forecasts that result from combining both datasets also indicate synergistic benefits. Overall, superior track and intensity forecasts are evident. This study suggests that polar-orbiting satellite spatial coverage should be considered in operational reconnaissance mission planning in order to achieve further improvements in TC analyses and forecasts.

1. Introduction

The Global Hawk (GH) is an unmanned aircraft system (UAS) that both the National Oceanic and Atmospheric Administration (NOAA) and the National Aeronautics and Space Administration (NASA) have utilized in many tropical cyclone (TC) field programs, including NASA's Genesis and Rapid Intensification Processes (GRIP; [Braun et al. 2013](#)) and Hurricane and Severe Storm Sentinel (HS3) experiments ([Braun et al. 2016](#)) and NOAA's Sensing Hazards with Operational Unmanned Technology field campaigns (SHOUT; [Black et al. 2014](#)). The GH is a long-endurance aircraft (up to 24 h) that can be equipped with multiple scientific instruments to collect data in the TC's inner-core and near-environment regions from high altitudes [16 750–19 800 m (55 000–65 000 ft)]. The data collected from the

GH, such as profiles of temperature, humidity, and winds from global positioning system (GPS) dropwindsondes (dropsondes hereafter; [Hock and Franklin 1999](#)), have been assimilated in both regional and global numerical weather prediction (NWP) models, and the results thus far show that they help improve predictions of both TC track and intensity ([Christophersen et al. 2017](#); [Howard et al. 2017](#)). Remote sensing instruments on board the GH such as the High-Altitude Imaging Wind and Rain Airborne Profiler (HIWRAP; [Heymsfield et al. 2013](#)) have also been shown to have positive impacts on both TC analyses and forecasts ([Sippel et al. 2014](#)).

While some studies have assessed the impact of assimilating GH observations in NWP models, little research has been conducted to evaluate the joint impact of GH observations and satellite observations. This is a valid research question because GH flight tracks and sampling strategies can, in theory, be modified to take advantage of a priori knowledge of the spatial and temporal data coverage from polar-orbiting satellites

Corresponding author: Hui Christophersen, hui.christophersen@noaa.gov

within the target region of interest. However, current planning of aircraft reconnaissance operations takes little or no consideration of existing satellite coverage, which is typically not the primary focus of the NOAA field campaigns (e.g., Rogers et al. 2006). Thus, if improved analyses and forecasts could be obtained by the joint assimilation of satellite and aircraft observations, the operational design of the flight tracks in reconnaissance and research missions could conceivably take advantage of known satellite orbits and plan accordingly.

In a global or regional data assimilation (DA) system, observations from different platforms can be assessed either by the forecast sensitivity to observations (FSO) technique (Langland and Baker 2004; Liu and Kalnay 2008) or through observing system experiments (OSEs). Both techniques are routinely used to evaluate the impact from one individual platform or multiple platforms at a time (e.g., McNally 2012; Majumdar et al. 2013; Lord et al. 2016) and generally obtain consistent results on the relative importance of each observation source for the same DA system (Gelaro and Zhu 2009). This study explores the joint impact of GH dropsondes and satellite observations using OSEs in a regional DA and forecast model. In particular, polar-orbiting satellites are considered because their overpasses in specific regions usually only occur once or twice daily.

2. Overview and procedures

a. Model initialization and forecast models

At the NOAA/Atlantic Oceanographic and Meteorological Laboratory/Hurricane Research Division (AOML/HRD), the Hurricane Ensemble Data Assimilation System (HEDAS) is one of the DA systems used for model initialization. It is a high-resolution vortex-scale DA system that employs the ensemble square root Kalman filter (Whitaker and Hamill 2002). It also provides the capability of processing and assimilating data within a storm-relative framework (Aksoy 2013). HEDAS includes a research version of NOAA's Hurricane Weather Research and Forecasting Model (HWRF; Gopalakrishnan et al. 2012; Atlas et al. 2015) that consists of an outer fixed domain with 9-km grid spacing and a 3-km vortex-following $10^\circ \times 10^\circ$ inner domain. Detailed physics configuration and model evaluation are described in Gopalakrishnan et al. (2012) and Yeh et al. (2012). The DA is only performed on the inner domain. The detailed configuration of the DA and the model for current experiments is described in Christophersen et al. (2017). Specifically, observations within a 6-h time window are processed and assimilated within a storm-relative framework, as in Aksoy (2013). The ensembles use the

first 30 out of 80 members of NOAA's ensemble-based Global Forecast System analyses (Hamill et al. 2011) as the initial and boundary conditions. A 4-h spinup and 4-h DA cycling (± 2 h of the synoptic time at 30-min cycles) are performed for each case. Five-day deterministic forecasts for each case are then run from the ensemble mean analysis.

b. Case description and observations

Cycling DA experiments are performed for a total of 18 cases (Table 1) with available dropsonde observations, 12 of which are from the 2012–14 HS3 field campaign and the rest from the 2015–16 SHOUT field campaign. In addition to dropsonde observations, the bulk of available observations are atmospheric motion vectors (AMVs; Velden et al. 2005) from the Geostationary Operational Environmental Satellite (GOES) and the Atmospheric Infrared Sounder (AIRS) cloud-cleared standard temperature and moisture retrievals (Susskind et al. 2003). Other datasets that are always assimilated when available are Constellation Observing System for Meteorology, Ionosphere and Climate (COSMIC) GPS radio occultation (RO) retrieved profiles (Kuo et al. 2004), nearby rawinsondes, and flight-level data from the Aircraft Communications Addressing and Reporting System (ACARS). However, the percentages of the other conventionally available datasets (GPS RO retrieved profiles, rawinsondes, and ACARS flight-level data) in total account for a very small portion of overall observations (4.5% on average over all cases; not shown). Observations from crewed reconnaissance aircraft, particularly tail Doppler radar (TDR) data, were shown by Christophersen et al. (2017) to be critical in representing the storm structure, but not all cases here have such data available. Therefore, to homogeneously compare the impact from GH dropsondes and/or AIRS, all crewed reconnaissance aircraft observations were excluded from assimilation in all experiments.

The experiments are designed as follows. The control (CNTL) experiment assimilates only the AMV retrievals and the "other" datasets. The AIRS experiment adds AIRS retrievals to the CNTL, the DROP experiment adds GH dropsondes to the CNTL, and the BOTH experiment adds both GH dropsondes and AIRS retrievals to the CNTL (Table 2).

Examination of the AIRS retrievals shows that there are large uncertainties associated with the observations in the upper troposphere and lower stratosphere. Further diagnosis in observation space also reveals that there are large root-mean-square errors and standard deviations associated with the observations above 100 hPa (not shown). To eliminate potential negative impacts from these upper-atmospheric retrievals, we only assimilate AIRS observations below 100 hPa in all experiments.

TABLE 1. Summary of the eight TCs that were examined, including each case initial time, initial best track intensity, and the peak intensity over the 5-day forecast.

Storm name	Initial time	Initial best track intensity (kt)	Peak intensity over the 5-day forecast (kt)
Nadine (2012)	0600 UTC 15 Sep	70	70
	0600 UTC 20 Sep	50	55
	0600 UTC 23 Sep	50	65
	1800 UTC 26 Sep	50	80
Humberto (2013)	0600 UTC 17 Sep	35	40
Cristobal (2014)	0600 UTC 29 Aug	70	70
Edouard (2014)	0600 UTC 12 Sep	35	105
	1800 UTC 14 Sep	75	105
	0600 UTC 15 Sep	85	105
	1800 UTC 16 Sep	95	95
	0600 UTC 17 Sep	85	85
Gaston (2016)	1800 UTC 18 Sep	65	65
	0600 UTC 27 Aug	55	105
Karl (2016)	1800 UTC 23 Sep	50	60
Hermine (2016)	0600 UTC 30 Aug	30	70
	0600 UTC 1 Sep	50	70
	1800 UTC 1 Sep	65	70
Matthew (2016)	1800 UTC 1 Sep	65	70
	1900 UTC 5 Oct	105	120

We further note that the dry bias in the GH dropsondes before the year 2016 (Vömel et al. 2016) will not impact the analyses presented in this study due to relatively large observation errors assigned to dropsonde humidity observations in the DA system (Christophersen et al. 2017).

3. Results

The vertical and horizontal data distributions for the AMVs, AIRS, and GH dropsondes are shown in Fig. 1. For the radius–pressure distribution, most of the AMV retrievals occur away from the storm center ($>\sim 300$ -km radius) and are concentrated in the upper troposphere, where the radial outflow is typically located, and above the planetary boundary layer, where a combination of GOES visible and shortwave IR channels tend to detect relatively large numbers of AMVs. The AIRS retrievals are concentrated mostly in the upper troposphere where it is typically clear or has thin cirrus and are clustered far away from the storm center ($>\sim 300$ km). On the other hand, GH dropsondes provide a more uniform radial distribution of data from inner-core observations ($<\sim 150$ km) out to the peripheral environment (~ 150 – 500 km) and are found throughout the atmospheric column up to the flight level. Horizontally, most of the AMV and AIRS retrievals are concentrated in the near environment of the storm, while GH dropsondes are clustered near the center of the storm, which illustrates that GH dropsondes complement AMV and AIRS retrievals azimuthally. It is further noted that on a

case-by-case basis, the complementary nature of AIRS and GH dropsonde sampling is even more pronounced (not shown).

The impacts on the analyses from the four experiments are shown in Figs. 2 and 3. Assimilating AIRS in addition to AMVs (AIRS experiment) does not seem to result in any obvious impact on the TC position or intensity on average, while combining GH dropsondes and AMVs (DROP experiment) shows a clear reduction in both the mean and median of the TC initial-time position and intensity errors. Using both GH dropsondes and AIRS in addition to AMVs (BOTH experiment) shows a further reduction. The improvements of the mean (median) of the position errors relative to the CNTL experiment for the DROP and BOTH experiments are 14% (30%) and 17% (39%), respectively. Only the median of the intensity error is further improved relative to the CNTL for BOTH (34%) compared to the DROP experiment (25%).

Similarly, the AIRS experiment has little impact on the initial-time mean storm structure (Figs. 3a,d,g), while the DROP experiment results in a slightly

TABLE 2. Summary of the experiment setup and assimilated datasets. All experiments also assimilate the other conventionally available observations including those from COSMIC and ACARS.

Expt	Assimilated datasets
CNTL	AMV retrievals
AIRS	AMV retrievals and AIRS retrievals
DROP	AMV retrievals and GH dropsondes
BOTH	AMV retrievals, AIRS retrievals, and GH dropsondes

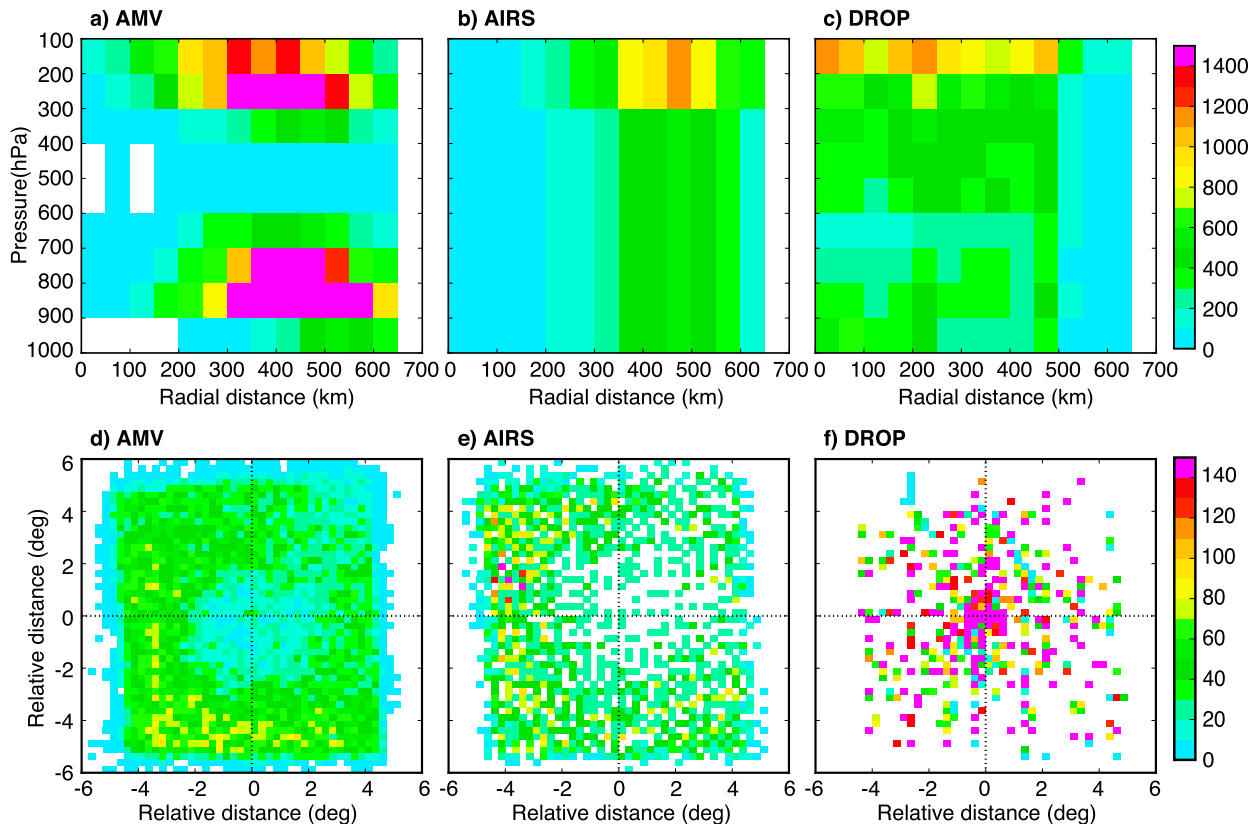


FIG. 1. (a)–(c) Radius–pressure frequency distribution and (d)–(f) horizontal frequency distribution of AMVs, AIRS, and GH dropsonde observations for the storms listed in Table 1. The color in each bin [50 km horizontally and 100 hPa vertically in (a)–(c), 0.25° longitudinally and 0.25° latitudinally in (d)–(f)] represents the number of observations accumulated over all cases. Radius/distance is measured relative to the storm center.

stronger primary circulation with the largest impact mostly concentrated within 100 km of the storm center radially and in the lowest 5–12 km vertically (Fig. 3b). The DROP experiment alters the mean outflow (Fig. 3e) and warm-core anomaly (Fig. 3h) as well. It is interesting to note that the BOTH experiment (Figs. 3e,f,i) has thermodynamic and kinematic impacts that are greater than in either the DROP or AIRS experiments, which indicates that the nonlinear feedback in DA and cycling from mutually independent information content of both datasets results in better analyses and forecasts.

The forecast errors compared to the best track estimates for the four experiments are shown in Fig. 4. It is noteworthy that the BOTH experiment has some superior skill relative to the CNTL experiment for track forecasts throughout the 120-h lead time, while the DROP experiment only has some skill for track compared to the CNTL forecasts up to 72-h lead time (Fig. 4a). This indicates that the BOTH experiment is able to combine the advantages of the DROP and AIRS experiments for an overall better track prediction. The advantage of using both the dropsondes and AIRS is more apparent

for the minimum sea level pressure (MSLP) forecasts. The BOTH experiment has more skill relative to the CNTL MSLP forecasts than either the DROP experiment or the AIRS experiment throughout almost the entire 5-day forecast period (Fig. 4c). We note that the superior performance of the intensity forecast of the BOTH experiment in terms of the 10-m maximum 1-min sustained wind speed is somewhat mixed, which is not surprising due to the fact that the 10-m maximum 1-min sustained wind speed is usually highly variable (Vukicevic et al. 2014), especially with the current limited sample size. The improved MSLP forecasts of the BOTH experiment are largely attributed to the greater-than-additive impact on the analyses from AIRS and dropsondes, as seen in the effective reduction of the initial-time position and intensity errors. While dropsondes are likely to show direct impact on the TC intensity (since the impact is mostly in the TC inner core; Fig. 3), AIRS data show an indirect impact on TC intensity since AIRS provides valuable data in the near environments of TCs. Despite this, in the composite-mean sense, AIRS retrievals alone make little improvement to the initial-time

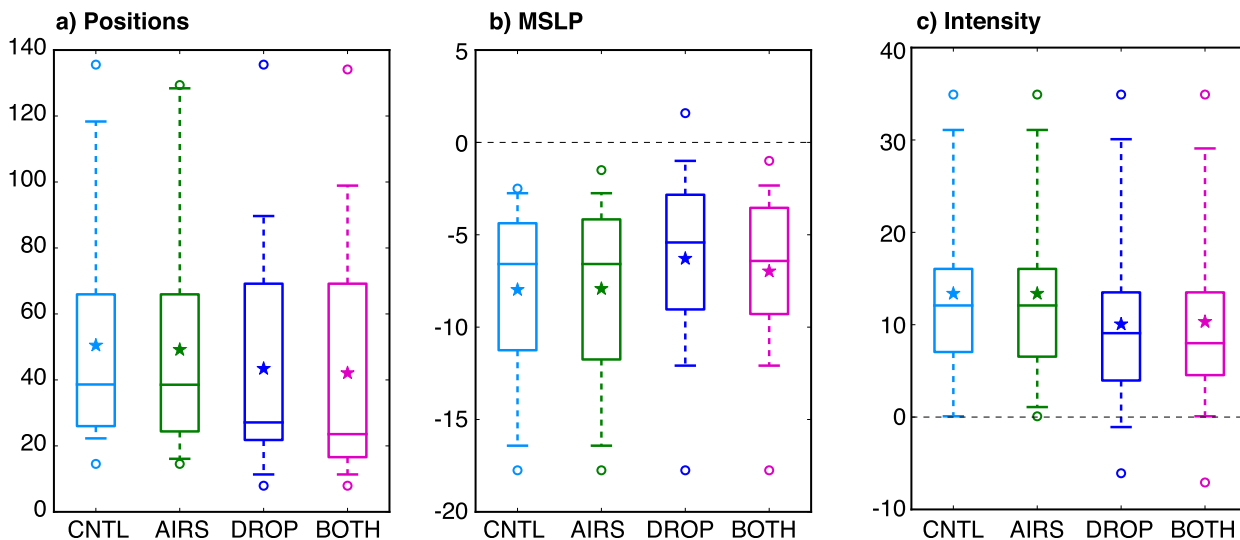


FIG. 2. Boxplots of initial-time position errors (km), MSLP errors (hPa), and intensity errors (m s^{-1}) (calculated as analysis minus best track estimates) for the analyses in the four experiments. The whiskers represent the 5th and 95th percentiles, and the circles are the outliers. The box extends from the 25th percentile to the 75th percentile of the data. The star symbols in each box denote the mean, and the horizontal lines in the box depict the median.

position, MSLP, or intensity (Fig. 2), or to the azimuthal-mean thermodynamic and kinematic structure (Fig. 3) relative to the CNTL. This is because the small yet potentially important contribution of the AIRS data to the initial-time TC structure and intensity is smoothed out over the cases investigated. Further examination on a case-by-case basis shows that the AIRS data have a modest impact on some TC initial-time intensity and structure. The magnitude of the impact is dependent predominantly on the data coverage and initial-time TC intensity. Furthermore, the pathways to regulate TC intensity by modifying near-environment thermodynamic conditions of TCs through DA can vary with many factors, such as vertical wind shear, sea surface temperature, TC initial intensity, and interactions with extratropical troughs and ridges (Holland and Merrill 1984; Tao and Zhang 2014; Munsell et al. 2013; Rios-Berrios and Torn 2017; Hanley et al. 2001). Hence, how AIRS data contribute to the improved MSLP forecasts varies greatly on a case-by-case basis.

Additionally, the BOTH experiment has more accurate track and intensity forecasts than the simple addition of the DROP and AIRS experiment during most of the 5-day lead time (Fig. 4), which is likely attributed to the synergistic benefits in the analysis. This encouraging result suggests that combining GH observations with satellite observations could achieve more than additive benefits for TC predictions, which demonstrates the importance of strategically designing aircraft flight

patterns that are coordinated with the satellite data coverage.

4. Demonstration of AIRS data impact: A case study

This section illustrates in a case study how AIRS data improve the MSLP forecasts when combined with GH dropsondes. It is cautioned that data impact varies significantly among cases in the available dataset due to variations in several factors, such as AIRS data coverage relative to aircraft observations, and storm initial-time intensity/structure.

At 0600 UTC 15 September, Hurricane Edouard (2014) was located at 26.5°N , 54°W with an intensity of 85 kt ($1 \text{ kt} = 0.51 \text{ m s}^{-1}$). The positions of the assimilated observations can be found in Christophersen et al. (2017) (Figs. 1a,b); AMVs and AIRS are mostly in the near environment of the TC, while GH dropsondes provide most of the inner-core sampling. The four experiments result in similar track forecasts, but different MSLP forecasts during the 5-day period (Figs. 5a,b). In particular, if we compare the DROP and BOTH experiments, BOTH shows a slight but consistent improvement in MSLP forecasts except at lead times of 36–48 h (Fig. 5c).

Further analysis reveals that assimilation of additional AIRS data in the BOTH experiment has a direct impact on the temperature anomaly and relative humidity structure in the TC simulation at the initial time (Fig. 6a)

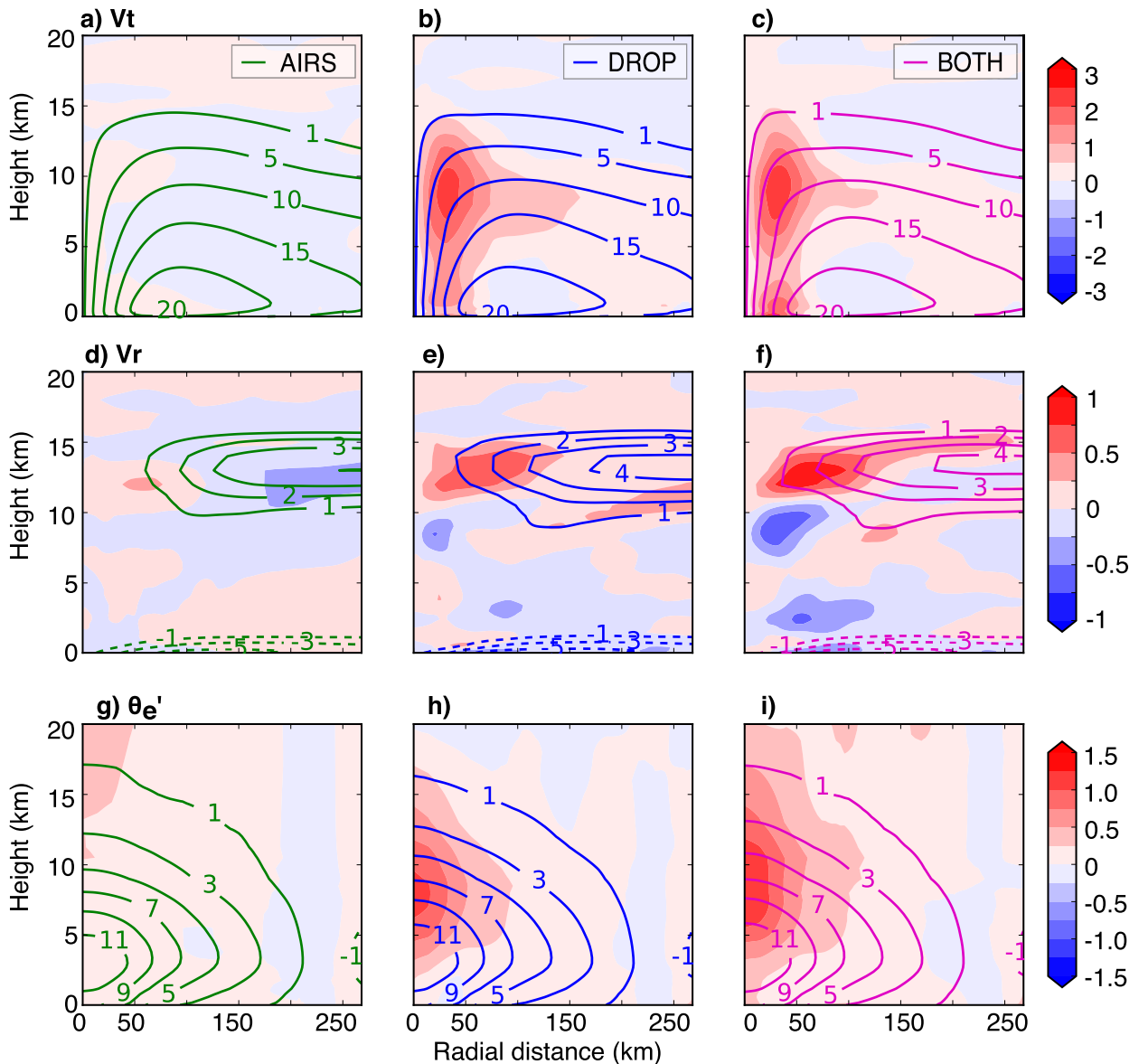


FIG. 3. Azimuthal means (contours) of (a)–(c) analysis tangential wind speed (m s^{-1}), (d)–(f) radial wind speed (m s^{-1}), and (g)–(i) equivalent potential temperature anomaly θ'_e (K) from the (left) AIRS, (center) DROP, and (right) BOTH experiments overlaid with differences with respect to the CNTL experiment (shaded).

and is associated with a stronger warm-core anomaly. Most of the thermodynamic differences between the DROP and BOTH experiments are located within 100 km of the TC center, which is likely through the covariances of the thermodynamic fields. Similarly, a noticeable impact on the kinematic fields in the analysis is seen (Fig. 6b), which is likely through strong correlations between thermodynamic and kinematics fields in mature TCs (Poterjoy and Zhang 2011). The small modifications of the temperature fields near the eyewall region (Fig. 6a) are likely to destabilize the atmosphere

and thus lead to more convection in that region of the storm. More active convection would lead to a broader and longer duration of condensational heating during forecasts in the BOTH experiment and hence produce a better-defined precipitation structure. As a response, more latent heat flux would be available for the TC to intensify in the BOTH experiment (Fig. 7). Such a scenario would be consistent with a decrease in the MSLP in the BOTH experiment relative to the DROP experiment during the 5-day forecasts (Fig. 5b), which is closer to the best track data. However, sensitivity

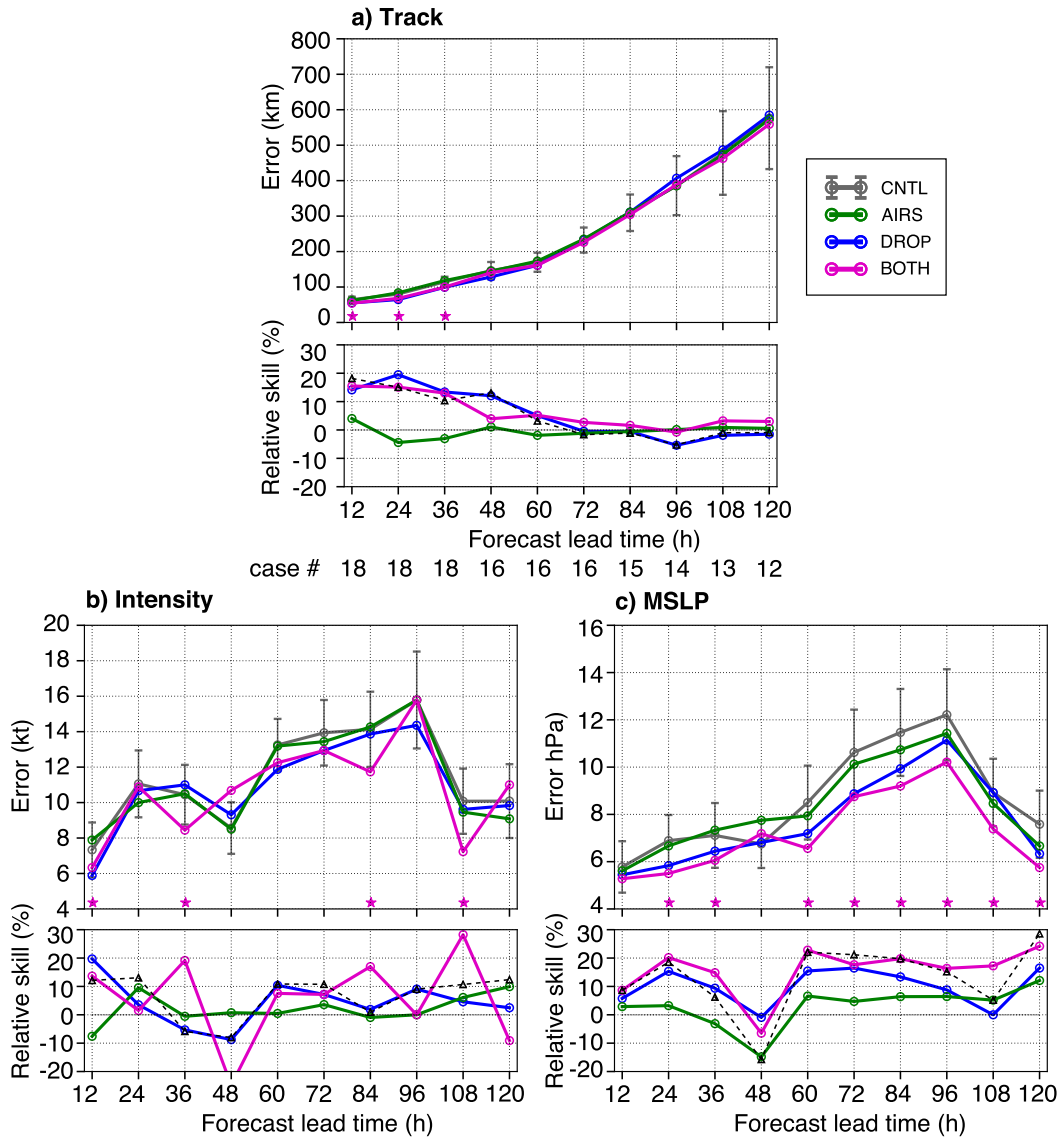


FIG. 4. Mean (a) track, (b) intensity, and (c) MSLP forecast errors for the CNTL, AIRS, DROP, and BOTH experiments and their skill relative to the CNTL experiment. The standard deviation of the mean errors in the CNTL experiment is shown by error bars in the top panels of (a)–(c). The summation of the relative skill from the AIRS and DROP experiments is also shown by the dashed black line in the bottom panels of (a)–(c). The BOTH experiment at a given lead time that is at least 90% statistically significantly different from the CNTL experiment is indicated by the purple star in the top panels of (a)–(c).

experiments beyond the scope of this study would be needed to evaluate whether this proposed modulation of the initial-time temperature or wind fields would lead to such variations in heating profiles and hence precipitation patterns during forecasts.

5. Conclusions and discussion

This study explores the potential of incorporating an optimal mix of satellite remote sensing observations

such as Atmospheric Infrared Sounder (AIRS) retrievals and aircraft in situ observations such as Global Hawk (GH) dropsondes into a regional ensemble data assimilation (DA) system for TC analysis and prediction. The database is derived from eight TCs that were sampled by the GH during the NASA HS3 and NOAA SHOUT field campaigns. Experiments are designed to assimilate geostationary satellite observations, such as atmospheric motion vectors (AMVs) in the control (CNTL) experiment, and adding AIRS

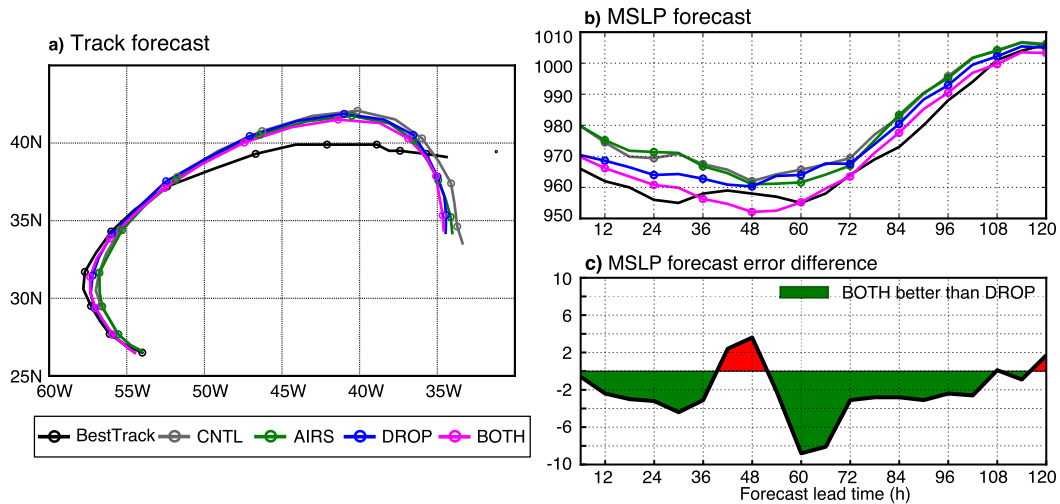


FIG. 5. The 124-h (a) track and (b) MSLP forecasts for Edouard (2014) initiated at 0600 UTC 15 Sep. The circles indicate every 12 h of lead time. (c) MSLP forecast error differences (hPa) between the BOTH and DROP experiments for the case of Edouard (2014) at 0600 UTC 15 Sep.

retrievals and/or GH dropsondes in the AIRS, DROP, and BOTH experiments. Data distributions show that AIRS observations in the near environment of the TC complement the inner-core regions that are typically well observed by GH dropsondes.

Average performance from all cases indicates that the BOTH experiment is more effective than the individual experiments in reducing the initial-time TC position and intensity errors. The analyses of mean TC structure demonstrate that the nonlinear feedback from both AIRS and dropsondes in the DA and cycling in the BOTH experiment contributes to more impact than

either dataset alone due to the assimilation of mutually independent information content. Specifically, the assimilation of dropsondes shows an impact on the TC inner-core structure, and the incorporation of AIRS observations helps to define the near environment of TCs. The greater-than-additive impact on the analyses in the BOTH experiment is believed to contribute to more accurate predictions of both the track and MSLP forecasts throughout most of the 5-day forecasts.

The results presented in this study admittedly are limited by sample size and hence lack statistical significance. We further note that because the AIRS

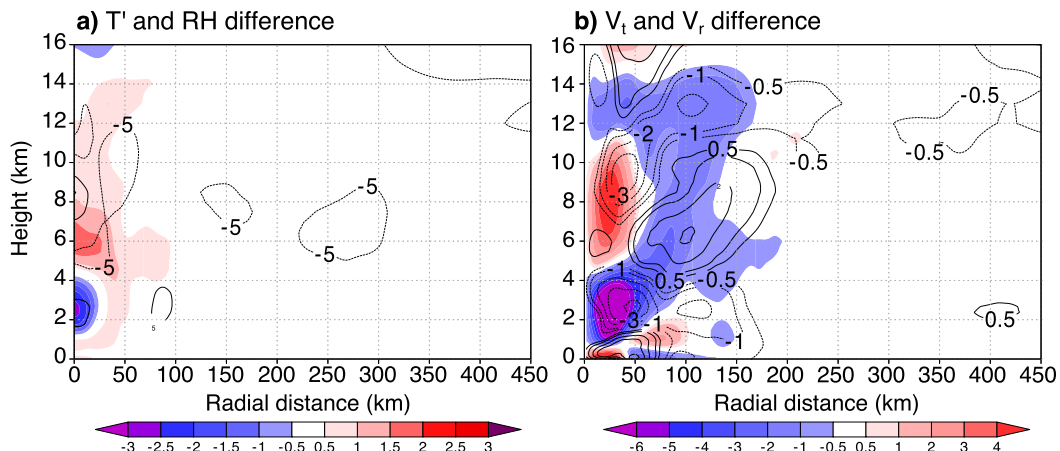


FIG. 6. (a) Temperature anomaly differences (K; shaded) and relative humidity differences (%; contours) of the final analysis between the BOTH and DROP experiments (BOTH minus DROP) for Edouard (2014) at 0600 UTC 15 Sep. (b) As in (a), but for tangential wind speed differences ($m s^{-1}$; shaded) and radial wind speed differences ($m s^{-1}$; contours).

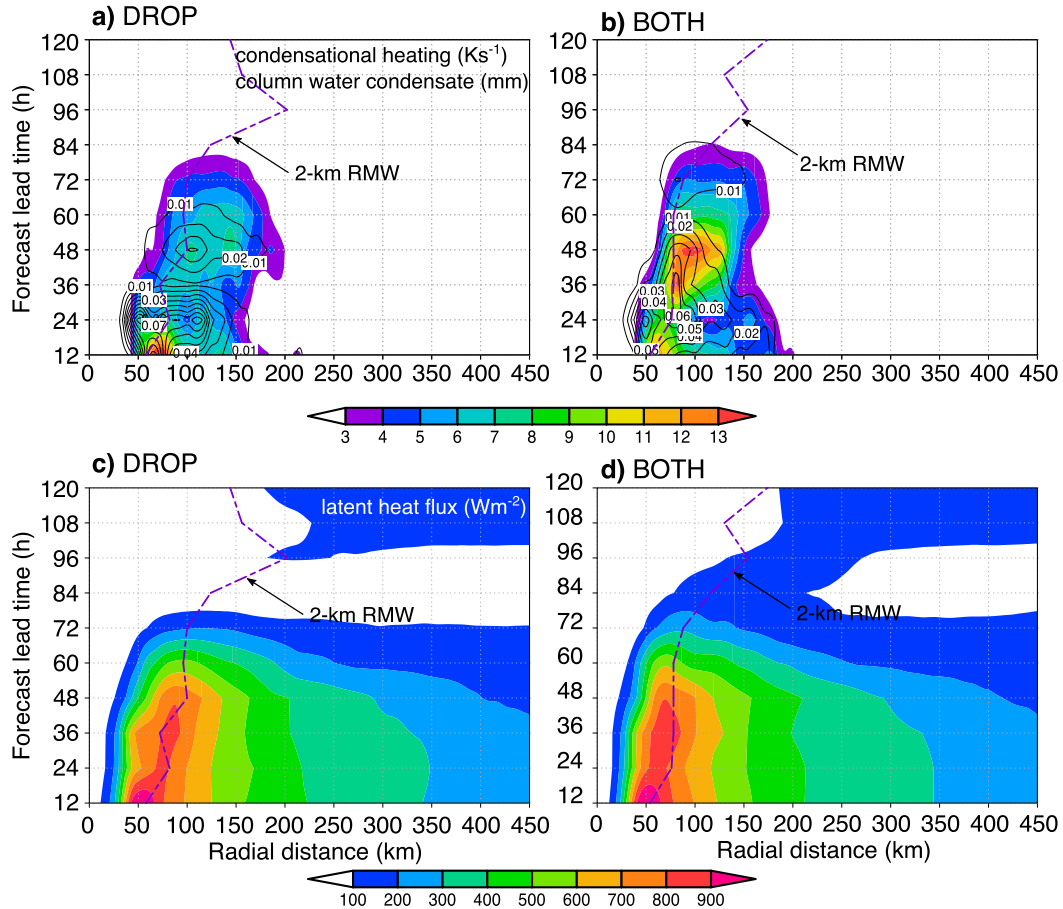


FIG. 7. (a),(b) Time–radius Hovmöller diagram of column-integrated condensational heating (contours) and water condensate (shaded) for Edouard (2014) initiated at 0600 UTC 15 Sep for the DROP and BOTH experiments. The radius of maximum wind (RMW) at 2 km indicated by the purple dashed line is calculated from the azimuthal mean of the tangential wind speed. (c),(d) Time–radius Hovmöller diagram of surface latent heat flux for Edouard (2014) initiated at 0600 UTC 15 Sep.

observations are cloud-cleared retrievals, they are mostly in the near environment of the storm regardless of the respective satellite orbit's proximity to the storm center. Another limitation of this study is that the dropsondes and AIRS data generally did not overlap spatially. More cases are needed to examine whether these datasets would be more effective if they overlapped spatially and temporally. Nonetheless, the results demonstrated here are encouraging and indicate the importance of coordination between aircraft and existing polar-orbiting satellite constellations for optimal TC sampling and prediction. This is particularly important given the limited observational resources (e.g., U.S. Air Force, NOAA, and Global Hawk aircraft) available during TC sampling. Careful allocation of resources based on both the economic and meteorological constraints needs to be addressed for a given case in order to achieve optimal tasking.

Acknowledgments. The authors acknowledge funding support from the NOAA UAS Program (Award NA14OAR4830172), and from the NOAA Hurricane Forecast Improvement Project (HFIP), which also provided the computing resources. The data used in this study were collected by the NASA HS3 field campaign (available online at https://espo.nasa.gov/hs3/content/HS3_0) and the SHOUT campaign (available online at ftp://ftp.aoml.noaa.gov/pub/hrd/data/global_hawk/). This research was carried out under the auspices of the Cooperative Institute for Marine and Atmospheric Studies, a joint institute of the University of Miami and NOAA (Cooperative Agreement NA67RJ0149). This manuscript was improved through careful internal review by Drs. Sim Aberson and Robert Rogers from NOAA/AOML/HRD and three anonymous reviewers. HC would like to thank Dave Nolan and Jon Zawislak, as well as the two internal reviewers, for their helpful discussions.

REFERENCES

- Aksoy, A., 2013: Storm-relative observations in tropical cyclone data assimilation with an ensemble Kalman filter. *Mon. Wea. Rev.*, **141**, 506–522, <https://doi.org/10.1175/MWR-D-12-00094.1>.
- Atlas, R., V. Tallapragada, and S. Gopalakrishnan, 2015: Advances in tropical cyclone intensity forecasts. *Mar. Technol. Soc. J.*, **49**, 149–160, <https://doi.org/10.4031/MTSJ.49.6.2>.
- Black, M., G. A. Wick, and R. E. Hood, 2014: Facing hazards with operational unmanned technology: NOAA's multi-year plan to deploy the NASA Global Hawk aircraft for high impact weather. *31st Conf. on Hurricanes and Tropical Meteorology*, San Diego, CA, Amer. Meteor. Soc., <https://ams.confex.com/ams/31Hurr/webprogram/Paper244777.html>.
- Braun, S. A., and Coauthors, 2013: NASA's Genesis and Rapid Intensification Processes (GRIP) field experiment. *Bull. Amer. Meteor. Soc.*, **94**, 345–363, <https://doi.org/10.1175/BAMS-D-11-00232.1>.
- , P. A. Newman, and G. M. Heymsfield, 2016: NASA's Hurricane and Severe Storm Sentinel (HS3) investigation. *Bull. Amer. Meteor. Soc.*, **97**, 2085–2102, <https://doi.org/10.1175/BAMS-D-15-00186.1>.
- Christophersen, H., A. Aksoy, J. Dunion, and K. J. Sellwood, 2017: The impact of NASA Global Hawk unmanned aircraft dropwindsonde observations on tropical cyclone track, intensity, and structure: Case studies. *Mon. Wea. Rev.*, **145**, 1817–1830, <https://doi.org/10.1175/MWR-D-16-0332.1>.
- Gelaro, R., and Y. Zhu, 2009: Examination of observation impacts derived from observing system experiments (OSEs) and adjoint models. *Tellus*, **61A**, 179–193, <https://doi.org/10.1111/j.1600-0870.2008.00388.x>.
- Gopalakrishnan, S. G., S. Goldenberg, T. Quirino, X. Zhang, F. Marks Jr., K.-S. Yeh, R. Atlas, and V. Tallapragada, 2012: Toward improving high-resolution numerical hurricane forecasting: Influence of model horizontal grid resolution, initialization, and physics. *Wea. Forecasting*, **27**, 647–666, <https://doi.org/10.1175/WAF-D-11-00055.1>.
- Hamill, T. M., J. S. Whitaker, D. T. Kleist, M. Fiorino, and S. G. Benjamin, 2011: Predictions of 2010's tropical cyclones using the GFS and ensemble-based data assimilation methods. *Mon. Wea. Rev.*, **139**, 3243–3247, <https://doi.org/10.1175/MWR-D-11-00079.1>.
- Hanley, D. E., J. Molinari, and D. Keyser, 2001: A composite study of the interactions between tropical cyclones and upper-tropospheric troughs. *Mon. Wea. Rev.*, **129**, 2570–2584, [https://doi.org/10.1175/1520-0493\(2001\)129<2570:ACSOTI>2.0.CO;2](https://doi.org/10.1175/1520-0493(2001)129<2570:ACSOTI>2.0.CO;2).
- Heymsfield, G. M., L. Tian, L. Li, M. McLinden, and J. I. Cervantes, 2013: Airborne radar observations of severe hailstorms: Implications for future spaceborne radar. *J. Appl. Meteor. Climatol.*, **52**, 1851–1867, <https://doi.org/10.1175/JAMC-D-12-0144.1>.
- Hock, T. F., and J. L. Franklin, 1999: The NCAR GPS dropwindsonde. *Bull. Amer. Meteor. Soc.*, **80**, 407–420, [https://doi.org/10.1175/1520-0477\(1999\)080<0407:TNGD>2.0.CO;2](https://doi.org/10.1175/1520-0477(1999)080<0407:TNGD>2.0.CO;2).
- Holland, G. J., and R. T. Merrill, 1984: On the dynamics of tropical cyclone structural changes. *Quart. J. Roy. Meteor. Soc.*, **110**, 723–745, <https://doi.org/10.1002/qj.49711046510>.
- Howard, K., J. Sippel, and V. Tallapragada, 2017: Impact of Global Hawk on GFS hurricane forecasts. *71st Interdepartmental Hurricane Conf.*, Miami, FL, Office of the Federal Coordinator for Meteorology, <https://www.ofcm.gov/meetings/TCORF/ihc17/2017presentations.htm>.
- Kuo, Y.-H., T. K. Wee, S. Sokolovskiy, C. Rocken, W. Schreiner, D. Hunt, and R. A. Anthes, 2004: Inversion and error estimation of GPS radio occultation data. *J. Meteor. Soc. Japan*, **82**, 507–531, <https://doi.org/10.2151/jmsj.2004.507>.
- Langland, R. H., and N. L. Baker, 2004: Estimation of observation impact using the NRL atmospheric variational data assimilation adjoint system. *Tellus*, **56A**, 189–201, <https://doi.org/10.1111/j.1600-0870.2004.00056.x>.
- Liu, J., and E. Kalnay, 2008: Estimating observation impact without adjoint model in an ensemble Kalman filter. *Quart. J. Roy. Meteor. Soc.*, **134**, 1327–1335, <https://doi.org/10.1002/qj.280>.
- Lord, S., G. Gayno, and F. Yang, 2016: Analysis of an observing system experiment for the Joint Polar Satellite System. *Bull. Amer. Meteor. Soc.*, **97**, 1409–1426, <https://doi.org/10.1175/BAMS-D-14-00207.1>.
- Majumdar, S. J., M. J. Brennan, and K. Howard, 2013: The impact of dropwindsonde and supplemental rawinsonde observations on track forecasts for Hurricane Irene (2011). *Wea. Forecasting*, **28**, 1385–1403, <https://doi.org/10.1175/WAF-D-13-00018.1>.
- McNally, A. P., 2012: Observing system experiments to assess the impact of possible future degradation of the Global Satellite Observing Network. ECMWF Tech. Memo. 672, 20 pp., <https://www.ecmwf.int/en/library/11085-observing-system-experiments-assess-impact-possible-future-degradation-global>.
- Munsell, E. B., F. Zhang, and D. P. Stern, 2013: Predictability and dynamics of a nonintensifying tropical storm: Erika (2009). *J. Atmos. Sci.*, **70**, 2505–2524, <https://doi.org/10.1175/JAS-D-12-0243.1>.
- Poterjoy, J., and F. Zhang, 2011: Dynamics and structure of forecast error covariance in the core of a developing hurricane. *J. Atmos. Sci.*, **68**, 1586–1606, <https://doi.org/10.1175/2011JAS3681.1>.
- Rios-Berrios, R., and R. D. Torn, 2017: Climatological analysis of tropical cyclone intensity changes under moderate vertical wind shear. *Mon. Wea. Rev.*, **145**, 1717–1738, <https://doi.org/10.1175/MWR-D-16-0350.1>.
- Rogers, R. F., and Coauthors, 2006: The Intensity Forecasting Experiment (IFEX): A NOAA multiyear field program for improving tropical cyclone intensity forecasts. *Bull. Amer. Meteor. Soc.*, **87**, 1523–1537, <https://doi.org/10.1175/BAMS-87-11-1523>.
- Sippel, J. A., F. Zhang, Y. Weng, L. Tian, G. M. Heymsfield, and S. A. Braun, 2014: Ensemble Kalman filter assimilation of HIWRAP observations of Hurricane Karl (2010) from the unmanned Global Hawk aircraft. *Mon. Wea. Rev.*, **142**, 4559–4580, <https://doi.org/10.1175/MWR-D-14-00042.1>.
- Susskind, J., C. D. Barnett, and J. M. Blaisdell, 2003: Retrieval of atmospheric and surface parameters from AIRS/AMSU/HSB data in the presence of clouds. *IEEE Trans. Geosci. Remote Sens.*, **41**, 390–409, <https://doi.org/10.1109/TGRS.2002.808236>.
- Tao, D., and F. Zhang, 2014: Effect of environmental shear, sea-surface temperature, and ambient moisture on the formation and predictability of tropical cyclones: An ensemble-mean perspective. *J. Adv. Model. Earth Syst.*, **6**, 384–404, <https://doi.org/10.1002/2014MS000314>.
- Velden, C. S., and Coauthors, 2005: Recent innovations in deriving tropospheric winds from meteorological satellites.

- Bull. Amer. Meteor. Soc.*, **86**, 205–223, <https://doi.org/10.1175/BAMS-86-2-205>.
- Vömel, H., K. Young, and T. F. Hock, 2016: NCAR GPS dropsonde humidity dry bias. NCAR Tech. Note NCAR/TN-531+STR, 8 pp., <https://doi.org/10.5065/D6XS5SGX>.
- Vukicevic, T., E. Uhlhorn, P. Reasor, and B. Klotz, 2014: A novel multiscale intensity metric for evaluation of tropical cyclone intensity forecasts. *J. Atmos. Sci.*, **71**, 1292–1304, <https://doi.org/10.1175/JAS-D-13-0153.1>.
- Whitaker, J., and T. M. Hamill, 2002: Ensemble data assimilation without perturbed observations. *Mon. Wea. Rev.*, **130**, 1913–1924, [https://doi.org/10.1175/1520-0493\(2002\)130<1913:EDAWPO>2.0.CO;2](https://doi.org/10.1175/1520-0493(2002)130<1913:EDAWPO>2.0.CO;2).
- Yeh, K.-S., X. Zhang, S. G. Gopalakrishnan, S. Aberson, R. Rogers, F. D. Marks, and R. Atlas, 2012: Performance of the experimental HWRF in the 2008 hurricane season. *Nat. Hazards*, **63**, 1439–1449, <https://doi.org/10.1007/s11069-011-9787-7>.